Cavity Formation from Inclusions in Ductile Fracture

A. S. ARGON, J. IM, AND R. SAFOGLU

The previously proposed conditions for cavity formation from equiaxed inclusions in ductile fracture have been examined. Critical local elastic energy conditions are found to be necessary but not sufficient for cavity formation. The interfacial strength must also be reached on part of the boundary. For inclusions larger than about 100Å the energy condition is always satisfied when the interfacial strength is reached and cavities form by a critical interfacial stress condition. For smaller cavities the stored elastic energy is insufficient to open up interfacial cavities spontaneously. Approximate continuum analyses for extreme idealizations of matrix behavior furnish relatively close limits for the interfacial stress concentration for strain hardening matrices flowing around rigid non-yielding equiaxed inclusions. Such analyses give that in pure shear loading the maximum interfacial stress is very nearly equal to the equivalent flow stress in tension for the given state of plastic strain. Previously proposed models based on a local dissipation of deformation incompatibilities by the punching of dislocation loops lead to rather similar results for interfacial stress concentration when local plastic relaxation is allowed inside the loops. At very small volume fractions of second phase the inclusions do not interact for very substantial amounts of plastic strain. In this regime the interfacial stress is independent of inclusion size. At larger volume fractions of second phase, inclusions begin to interact after moderate amounts of plastic strain, and the interfacial stress concentration becomes dependent on second phase volume fraction. Some of the many reported instances of inclusion size effect in cavity formation can thus be satisfactorily explained by variations of volume fraction of second phase from point to point.

It appears that Joseph Henry,[1] of electro-magnetism fame, has recognized as early as 1855 that metals fracture prematurely by a process of internal necking when extended by stretching. He advised that wire drawing and rolling were preferable operations (for this and other interesting historical perspectives on deformation processing see Backofen[2]). In more recent times Puttick[3] traced the cause of ductile fracture to the development of holes from inclusions (for a summary of earlier views on ductile fracture and their inadequacy see Orowan[4]). The process has since been investigated extensively both experimentally and theoretically. The current level of understanding of the role of inclusions in ductile fracture has been reviewed by Rosenfield.[5] It has now been generally established that once internal cavities are nucleated from inclusions or second phase particles, they can be plastically expanded under various combinations of shear stress and negative pressure. Analyses of homogeneous plastic cavitation by McClintock,[6] Rice and Tracy[7] and others have elucidated the importance of negative pressures in the flow field in hastening the plastic hole expansion process. Comparison of such analyses with experiments have shown that local ductile fracture requires considerably smaller average plastic strain as a result of localization of dilational deformation into zones,[8] followed by formation and propagation of cracks where the hole expansion process is sharply confined into portions of the highly strained zone in front of the crack.[9,10] Although these processes of terminal ductile separation are not yet fully understood, they are in a far better level of development than the initial processes which lead to the nucleation of holes from second phase inclusion particles.[5] On the experimental side there have been conflicting observations reporting the nucleation of cavities from inclusions anywhere from immediately upon yielding to after the development of very large plastic strains. Cavities have been reported to nucleate both on interfaces by tearing the inclusion away from the ductile matrix, and by cracking of non-deformable inclusions. On the other hand semi quantitative theoretical studies have been made, based on release of stored elastic energy,[11,12] production of high stresses by impingement of dislocation pile-ups on inclusions,[11,13] and by reverse pile-ups of plastic accommodation loops initiated by punching from the interface.[14] More phenomenological models have also been advanced based on the development of high local shear strains at particle interfaces.[15] Here we will briefly review these mechanisms of cavity nucleation and present new analytical developments on a local stress criterion of interfacial separation. In the accompanying paper[16] we compare the results of experiments on a number of inclusion-bearing metals with these new analytical developments.

A. S. ARGON is Professor of Mechanical Engineering and J. IM is Graduate Student at the Massachusetts Institute of Technology, Cambridge, Mass., 02139. R. SAFOGLU is with the Department of Mining and Metallurgy, Technical University of Instanbul, Istanbul, Turkey. This work has been presented in part orally at the Third International Conference on Fracture in Munich, Germany, April 1973.

Manuscript submitted November 5, 1973.

1. CRITERIA FOR INCLUSION SEPARATION

1.1. Assessment of Earlier Developments

Although it has generally been recognized that some plastic strain is necessary to form holes at inclusions,

most quantitative developments for ductile fracture have compared experimentally measured strains to fracture with theoretically computed strains for hole growth and coalescence.[17,7] There are many observations, however, which show that most often large plastic strains are required to tear inclusions free, or produce internal fracture in them.[18-20] Hence we assume together with most of the former workers who have considered the problem of cavity nucleation that such holes are a result of a more or less extensive pre-processing. It has been generally observed that while inclusions with large aspect ratio may undergo multiple internal fracturing, equiaxed inclusions almost always nucleate holes by interfacial separation. *Here we confine our attention only to the equiaxed inclusions which we will consider as a first approximation as rigid and plastically non-deformable.* The problem of non-equiaxed inclusions, whose behavior depends on their shape and orientation in addition to their size and spacing is a complex one and will not be discussed here.

As already mentioned in the previous section, the earlier considerations of inclusion separation can be grouped into three categories, energy criteria, local stress criteria, and local strain criteria.

Gurland and Plateau[11] proposed that cracks at interfaces could form when the locally concentrated elastic strain energy which could be released upon decohesion becomes comparable to the energy of the surfaces to be generated. Considering no local plastic accommodation and without investigating whether or not the stored elastic energy could actually be released by crack formation, they based their arguments on dimensional analysis and concluded that cracks would form at lower applied stresses on large inclusions. As pointed out by Brown and Stobbs[20] the analysis of Gurland and Plateau is only a necessary condition for inclusion separation. A more correct analysis by Tanaka, Mori, and Nakamura[12] has shown that in a purely elastic situation, the energy criterion is always satisfied for particles above a diameter of about 250Å, almost upon yielding. Since in many instances inclusions of more than hundred times this size have been observed to remain attached to the matrix at strains more than hundred times the yield strain it must be concluded that the energy requirement is only a necessary one and that actual separation requires reaching the interfacial strength at the interface, at least at some local points, to provide a nucleus of separation. It must then follow that for very small particles of diameter much less than the critical diameter of 250Å where the energy criterion may not be satisfied even when local stresses reach the interfacial strength, stable cavities are difficult to form. The interface would merely separate a distance of the order of atomic dimensions relieving much of the elastic strain energy but still transmitting some long range attractive forces. Cavities could then still form very gradually and in a stable manner as the local displacement incompatibilities at the interface continue to increase with increasing average plastic strain. Similar problems of this nature related to the very short range singular stress fields around dislocation cores have been discussed by Stroh.[21]

Gurland and Plateau[11] and also Broek[13] have attributed cavity formation to impingement of dislocation pile-ups at inclusions in the manner proposed by Zener[22] and analyzed by Stroh.[23] At low temperature where slip tends to be planar, cavities can be produced by this mechanism especially if the inclusions have a large aspect ratio increasing the probability for them to interfere with such planar slip. Some of the observations on the splitting of elongated inclusions is probably due to this mechanism. At moderate temperatures in close packed metals where many equivalent slip systems become operable and slip tends to become wavy, the ease of secondary slip will make the development of high stresses difficult or almost impossible. Therefore, in ductile fcc metals and even in bcc metals at moderate temperatures this mechanism is almost certainly not responsible for cavity formation around inclusions. Ashby[14] has discussed an interesting alternative in which primary deformation incompatibilities do not produce cavities directly, but initiate highly organized secondary slip by punching out dislocation loops from the interface of the inclusion with the matrix to reduce the local shear stresses. These loops then form reverse pile-ups and can build up increasing interfacial tensile stresses until they reach the interfacial strength when a cavity is formed. Ashby's model amounts to a special upper bound analysis for plastically dissipating primary deformation incompatibilities; it is however not an upper bound analysis for the total problem since the assumed flow field is only local and does not satisfy the distant deformation boundary conditions of the entire body. Ashby has shown that this model can also be formulated completely as a macroscopic slip line field in which positive and negative deformation incompatibilities around the particle can be balanced against each other by a closed slip line field of four lobes.[24] Thus, in spite of the fact that the interfacial stresses calculable by this model are no better than a high upper bound, the model is conceptually simple and as we will show later is useful in understanding interactions between particles to explain why large particles lead to cavity formation before small particles.

McClintock[15] has given an extensive elastic-plastic continuum analysis of stress distributions around cylindrical particles in anti-plane strain, where it is shown that large strain concentrations can develop around non-deforming particles in non-strain hardening matrices. Arguing that similar strain concentrations must also occur in plane strain deformation and that such high strain concentrations in crystal plasticity are usually composed of dislocation pile-ups, McClintock has suggested that cavity formation at interfaces may obey a critical local strain criterion, or alternatively a criterion that may be a mixture of a critical interfacial shearing strain and an interfacial normal stress. The nature of this combined criterion has not been clarified. Most investigators have adopted one of the above criteria to explain their results.

Below we will consider the separation primarily of only large particles for which the energy criterion is always satisfied and cavity formation can be expected to depend on reaching locally a critical interfacial tensile strength.

1.2 Critical Stress Criteria Based on Continuum Deformation

In most instances ductile fracture results from cavities formed around inclusions of micron size. On the

other hand, transmission electron microscopy of dislocation structures around inclusions of sub-micron size have shown that the spacing of the surrounding dislocations in the high strain gradient zones are very much smaller than the particle diameter, (see *e.g.*, Ref. 18) suggesting that at least for large particles a continuum analysis of deformation is proper. On the other hand dislocation structures around small particles of only several hundred Angstroms diameter are usually highly organized prismatic loops,[20,25] requiring a more discrete dislocation analysis for the interfacial stresses.*

*In materials where strong slip bands can form due to a low stacking fault energy or due to some form of strain softening, the scale for continuum analysis will be of the order of these slip band lengths.

Below we will discuss both approaches in order.

Considering the particle as a rigid cylinder and the surrounding matrix as an elastic, plastic strain hardening continuum, the development of interfacial stresses is desired for pure shear deformation. The solution for any other state of deformation having a negative pressure component can then be obtained by superimposing this negative pressure on the interfacial stresses of the pure shear solution. Some solutions of this type already exist. Huang[26] has presented a deformation theory solution for a rigid cylindrical inclusion embedded into an incompressible Ramberg-Osgood (power-law) material with a stress exponent of 7. He finds that a strain independent, constant interfacial tensile stress concentration develops which is maximized at an angle of about 12 deg toward either side of the principal tension axis, and has a magnitude of 1.36 times the distant boundary shear traction. Huang also showed that for a decrease in the stress exponent corresponding to increasing strain hardening behavior the stress concentration increases steadily (and presumably approaches asymptotically the solution for an incompressible linear material). Orr and Brown[27] have considered the same problem in which the matrix was modelled as an incompressible elastic-plastic material with either no hardening or a linear hardening rate equal to 1/40 of the Young's modulus. Orr and Brown too find that the interfacial tensile stress reaches a maximum value away from the principal tensile direction but at an angle of about 17 deg toward either side of this direction. Unlike Huang, Orr and Brown find, however, that the magnitude of the interfacial tensile stress concentration increases steadily as the distant plastic strain increases both for the non-hardening as well as the hardening material, and shows little change in this behavior even at distant plastic strain levels 15 times the yield strain—in spite of the fact that a steady state might be expected from upper bound arguments for the non-hardening case. At that time the maximum interfacial stress is 2.52, and 3.03 times the boundary shear traction for the non-hardening and linearly strain hardening material respectively. Because of this difficulty of a lack of steady state for the non-hardening material even at large plastic strains, we find the solution of Orr and Brown not very useful.

Rhee and McClintock[28] have demonstrated by means of a number of specific examples that the strain concentrations in inhomogeneous deformation fields in strain hardening materials can be bounded by two limiting idealizations of the plastic behavior of the material: a non-hardening rigid plastic behavior and a linear behavior with zero yield stress as shown in Fig. 1. Assuming that the same idea may also extend to stress

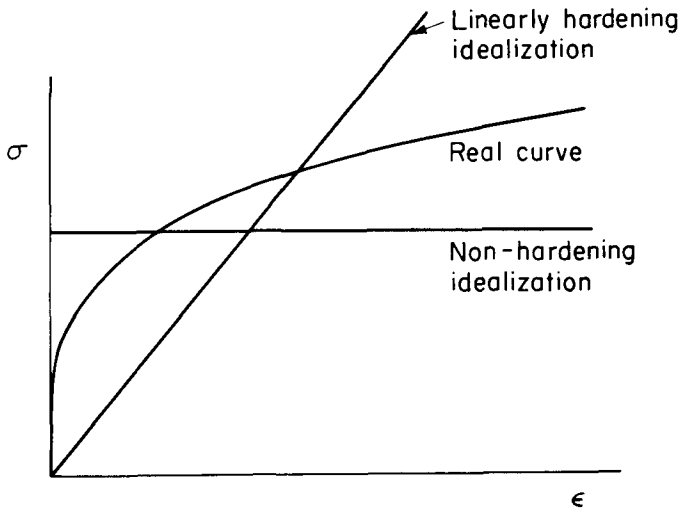

Fig. 1—Idealization of actual plastic behavior by two limiting forms of non-hardening rigid plastic, and linear behavior.

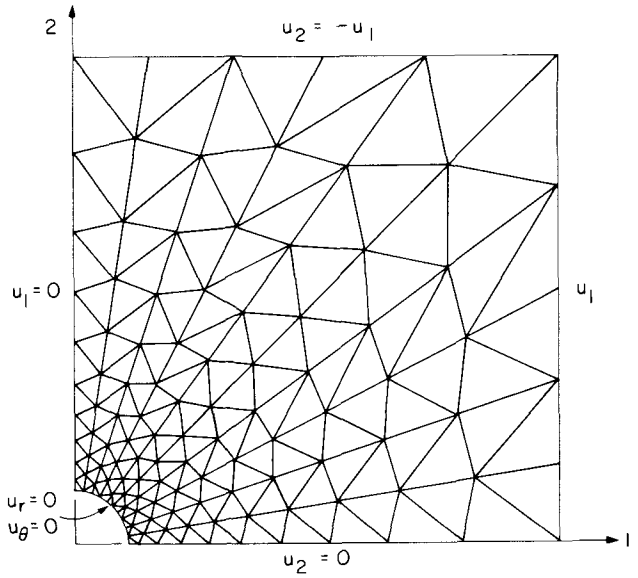

Fig. 2—One quadrant of grid for finite element solution of initiation of plastic flow in pure shear around a rigid cylinder.

concentrations we have obtained a finite element solution for the pure shear deformation of an elastic-ideally plastic, non-hardening continuum around a rigid cylindrical inclusion and compared this with the available linear solution as the other form of extreme idealization.

The chosen net configuration for the finite element solution corresponding to 0.01 volume fraction of second phase is shown in Fig. 2. The elastic-plastic program of Marcal and King[29] was used for six increments of constant tensile and compressive boundary displacements equivalent to pure shear, starting from the point where some elements in the chosen network just become plastic. The solution was obtained for conditions representative for a ductile metal such as aluminum (or copper), *i.e.*, for a Young's modulus of 10^4 ksi, a Poisson's ratio of 1/3, and a yield stress in tension of 1.6 ksi, giving $\epsilon_y = 1.6 \cdot 10^{-3}$. The spreading of the plastic zones with these increments is shown in Figs. 3(*a*) through (*e*) as the shaded regions. The computed interfacial tensile stresses and tangential shear strains around the inclu-

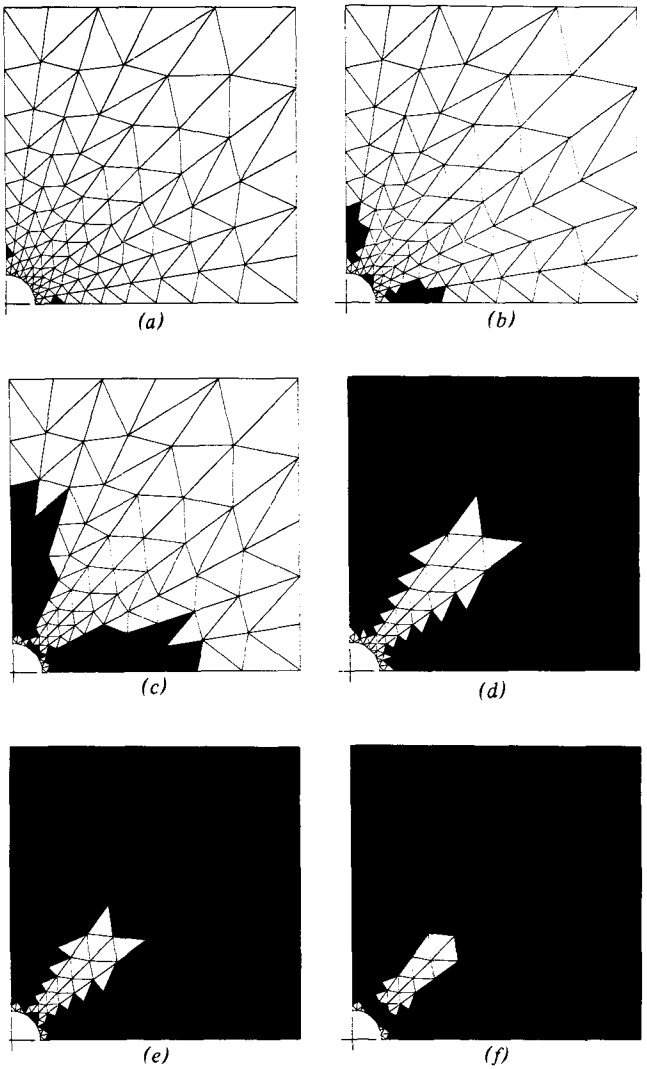

Fig. 3—Spreading of the plastic region (shaded) with increasing boundary displacements for elastic, non-hardening plastic idealization: (*a*) $u_1 = u_0$ where plastic flow is just initiated, (*b*) $u_1 = 1.1u_0$, (*c*) $u_1 = 1.2u_0$, (*d*) $u_1 = 1.3u_0$, (*e*) $u_1 = 1.4u_0$, (*f*) $u_1 = 1.5u_0$.

sion as a function of an angle θ measured from the direction of principal tension are given in Tables Ia through c. Unlike the two solutions discussed above our solution shows a flat maximum for the interfacial stress in the principal tensile direction without a significant drop before an angle of about 15 deg. Since the finite element net is quite coarse and other unevennesses of stress are apparent from Table I, we attribute this to defects in the program and accept the maximum interfacial stress at $\theta = 0$ deg as an appropriate measure of the concentrated interfacial tensile stress. The change of this maximum stress in units of the yield strength in shear k of the matrix is given as a function of the increasing distant shear strain in Fig. 4, and indicates that a fairly stable solution was reached. The maximum interfacial tensile stress is found to be $1.5k$ which is somewhat higher than the stress obtained by Huang. The distribution of equivalent shear strain which is mapped out by the spreading plastic zones shown in Fig. 3(*a*) through (*e*) resemble closely that obtained by Orr and Brown. We note further from Table Ic that there is only a very moderate interfacial shear strain concentration of about 1.10 on the interface parallel to the planes of maximum shear strain in the distant field (*i.e.*, at $\theta = 45$ deg).

Table Ia. Normalized Radial Stresses σ_{rr}/k Around the Inclusion, Measured From a Point under the Tensile Direction

	θ				
$\gamma/(k/G)$	4.5 deg	13.5 deg	22.5 deg	31.5 deg	40.5 deg
0.770	1.495	1.400	1.025	0.765	0.160
0.848	1.606	1.535	1.125	0.825	0.175
0.925	1.550	1.510	1.070	0.905	0.180
1.000	1.480	1.440	1.000	0.875	0.150
1.080	1.425	1.380	0.930	0.875	0.140
1.158	1.400	1.380	0.900	0.870	0.100

Table Ib. Normalized Tangential Stresses $\sigma_{\theta\theta}/k$ Around the Inclusion, Measured From a Point Under the Tensile Direction

	θ				
$\gamma/(k/G)$	4.5 deg	13.5 deg	22.5 deg	31.5 deg	40.5 deg
0.770	0.745	0.700	0.510	0.385	0.080
0.848	0.800	0.765	0.560	0.435	0.090
0.925	0.780	0.755	0.535	0.420	0.100
1.000	0.740	0.720	0.500	0.500	0.090
1.080	0.710	0.690	0.465	0.500	0.090
1.158	0.700	0.690	0.450	0.520	0.060

Table Ic. Magnitude of Normalized Tangential Shear Strain $\gamma_{r\theta}/(k/G)$ Around the Inclusion, Measured From a Point Under the Tensile Direction

	θ				
$\gamma/(k/G)$	4.5 deg	13.5 deg	22.5 deg	31.5 deg	40.5 deg
0.770	0.026	0.570	0.615	0.950	0.970
0.848	0.032	0.622	0.675	1.060	1.080
0.925	0.032	0.610	0.660	1.225	1.250
1.000	0.032	0.675	0.725	1.220	1.240
1.080	0.026	0.692	0.740	1.255	1.275
1.158	0.026	0.725	0.770	1.340	1.360

The second bounding solution for the interfacial stresses around a rigid inclusion in an incompressible (*i.e.*, $\nu = 0.5$) linear material can be obtained directly from the theory of elasticity (see Muskhelishvilli[30] or Savin[31] and are

$$\sigma_{rr} = p\left[4\left(\frac{\rho}{r}\right)^2 - 3\left(\frac{\rho}{r}\right)^4 + 1\right]\cos 2\theta \qquad [1]$$

$$\sigma_{\theta\theta} = p\left[3\left(\frac{\rho}{r}\right)^4 - 1\right]\cos 2\theta \qquad [2]$$

$$\sigma_{zz} = p\,2\left(\frac{\rho}{r}\right)^2\cos 2\theta \qquad [3]$$

$$\sigma_{r\theta} = p\left[2\left(\frac{\rho}{r}\right)^2 - 3\left(\frac{\rho}{r}\right)^4 - 1\right]\sin 2\theta \qquad [4]$$

where p is the boundary shear traction and ρ the radius of the cylinder. The interfacial tensile stresses and shear strains around the inclusion are plotted in Fig. 5 as a function of the angle θ. We see that the tensile stress is maximized at $\theta = 0$ and is equal to 2 times the boundary shear traction. Similarly the interfacial shear strain is maximized at $\theta = 45$ deg and is also equal to twice the distant boundary shear strain.

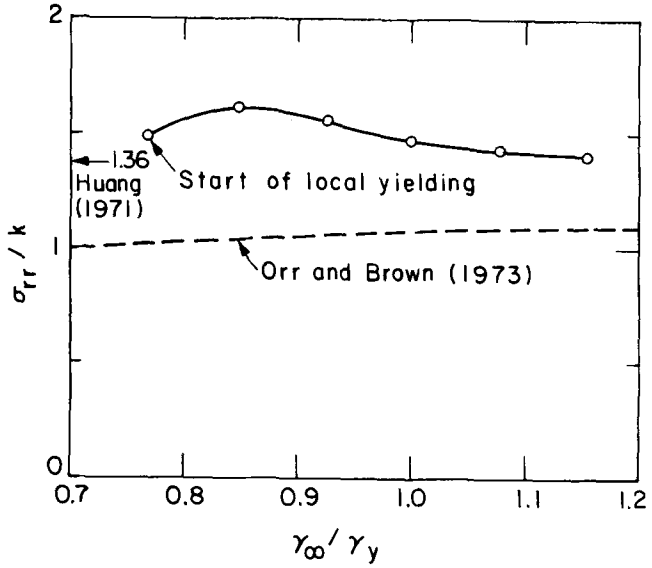

Fig. 4—Change of maximum interfacial tensile stress with increasing boundary strain in non-hardening material. Solutions of others are also shown for comparison.

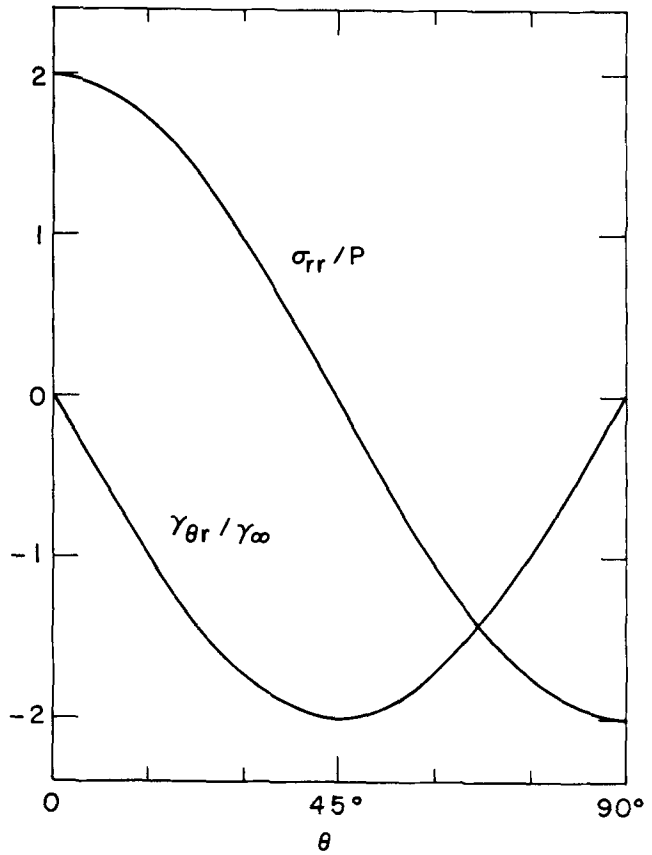

Fig. 5—Distribution of interfacial tensile stress and shear strain around a rigid particle in an incompressible linear matrix.

Fig. 6 shows the distribution of the total principal strain ϵ_{xx} outside the inclusion for the two bounding solutions, in units of the total distant strain. The solid curve represents the distribution obtained from the final increment in the finite element analysis, while the broken curve is computed from Eqs. [1] and [2] by means of the elastic stress strain relations, in which the local

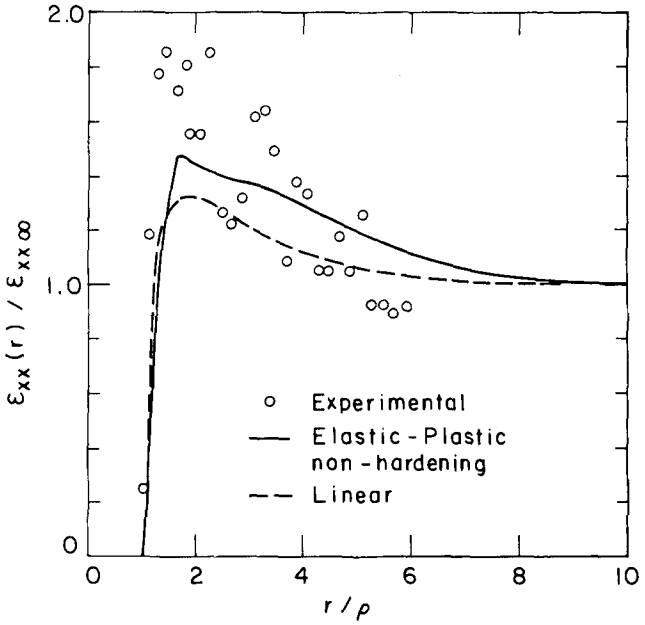

Fig. 6—The distribution of principal total strain ϵ_{xx} parallel to the tension direction for the elastic, non-hardening plastic material, the linear incompressible material, and experimental measurements on a model copper specimen with a hardened cylindrical Cu-Be "inclusion".

strains are again normalized with the distant strain $\epsilon_{xx\infty}$.

If the distant deformation field were not pure shear but had a negative pressure component σ_T, this negative pressure would have to be added to the plastic drag induced interfacial stresses computed by the two limiting solutions discussed above. Thus, based on Rhee and McClintock's hypothesis the actual interfacial stresses could now be bounded as

$$\tfrac{3}{2}k \leq \sigma_{rr} - \sigma_T \leq 2k \qquad [5]$$

where the left hand bound is for the non-hardening idealization while the right hand bound is for the linear idealization where k is considered as the *flow stress* in shear. If Huang's solutions for the Ramberg-Osgood material with power-law hardening were to be extrapolated to non-hardening behavior and were taken for the lower limit it may be as low as k. Since for most of the strain hardening behavior of interest, *i.e.*, for the exponents n between 2 and 8, Huang's solutions either fall slightly below the lower limit or between the limits, we will take the above limits as bounds for the plastic drag induced interfacial tensile stress. Since these limits are rather close together and since their mean value of $1.75k$ is very nearly the flow stress in tension, Y, we take for the total interfacial tensile stress

$$\sigma_{rr} \simeq Y(\bar{\epsilon}^p) + \sigma_T \qquad [6]$$

where $Y(\bar{\epsilon}^p)$ is the flow stress in the region of the inclusion for the average local plastic strain of the region, had the inclusion not been present.

Eq. [6] shows that the interfacial stress will increase with strain hardening and with triaxiality. Both of these effects are known to reduce ductility and hence, most likely, also promote cavity formation. The above continuum analysis for an isolated inclusion predicts an interfacial stress dependent only on the surrounding strain state and negative pressure but not on the size

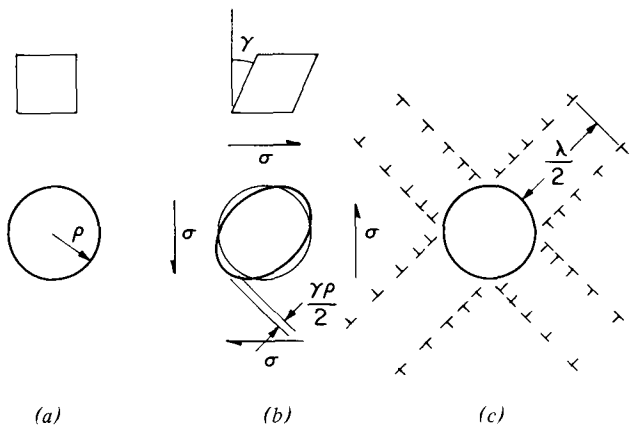

Fig. 7—Ashby's model of the production of a secondary plastic zone to dissipate the elastic shear stresses arising from the interfacial displacement incompatibility upon plastic straining of the matrix.

of the particle. We will see below that the particle size effects are a result of particle interactions which occur at large local second phase concentrations and at large plastic strains.

1.3 Critical Stress Criteria Based on Dislocation Models

In a study of enhanced work hardening due to non-deformable inclusions Ashby[14] proposed a plastic accommodation model of displacement incompatibilities which develop between a homogeneously shearing continuum and a rigid inclusion. This model which is particularly useful in the understanding of inclusion interactions is based on Eshelby's[32] approach for considering transformation problems. It is illustrated in Fig. 7. In a thought experiment the non-deformable spherical inclusion of radius ρ shown in Fig. 7(a) is removed and replaced by a sphere of parent material. The continuum is plastically sheared by an amount γ which distorts the sphere of parent material into an ellipsoid as shown in Fig. 7(b). The distorted ellipsoid is now removed and the non-deformable sphere is to be re-inserted. This requires the elimination of the displacement incompatibilities of a maximum amoung of $\gamma\rho/2$. For small shear strains such incompatibilities could be accommodated in the matrix by local elastic deformation. If the inclusion is very small and if the surrounding material lacks operable dislocation sources the elastic stresses could rise until the ideal shear strength is reached at the interface and dislocation loops are punched out to form a plastic accommodation zone shown in Fig. 7(c). This plastic accommodation zone reduces the shear stresses around the inclusion. The interfacial normal stresses, however, continue to rise to form a cavity across the principal tensile direction when the interfacial stress reaches the interfacial strength. Although this model is not a fully acceptable upper bound flow field for the reasons already given above, it is simple and lends itself to the incorporation of many important details. Therefore, we will develop it further.

We assume, together with Ashby, that the ideal shear strength is reached at the interface before the ideal cohesive strength of the interface (Kelly, Tyson, and Cottrell[33] have discussed the atomic bonding requirements in different materials for this condition to be satisfied) and that circular loops are punched out and moved away from the spherical inclusion against an effective shear drag k_s. We simplify the problem by considering the dislocation loops as a continuously distributed dislocation density and idealize the model as a cylindrical punch indenting an elastic-plastic cylinder either into or out of a cylindrical hole in a rigid semi-infinite medium against a wall frictional drag of amount k_s which can be taken as the critical resolved shear stress of yielding of a single crystal, as shown in Fig. 8(a). We find it necessary to distinguish a number of important alternatives.

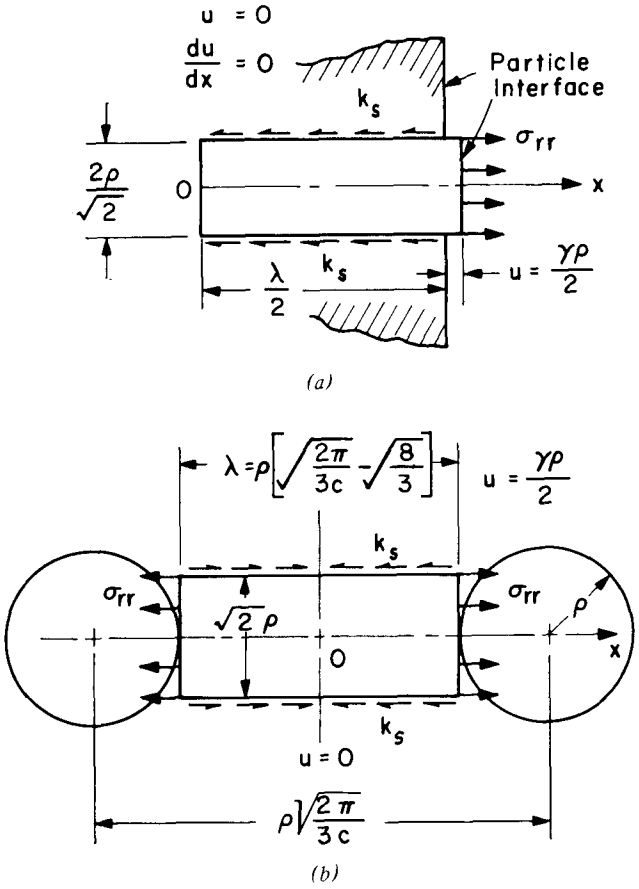

Fig. 8—(a) Idealization of the cylindrical plastic punching by a cylinder elastically or plastically extended in a rigid cavity against wall friction; (b) Plastic punching between two interacting particles.

a) Very small spherical inclusions ($\rho \leq 100$Å): The idealized model is as shown in Fig. 8(a). The cylinder of radius $\rho/\sqrt{2}$ is extracted outward (punched outward) by interfacial normal surface tractions σ_{rr} against only a wall friction, it contains no dislocations inside, hence is incapable of undergoing internal plastic relaxation.*

*The radii of the cylindrical secondary plastic zones are chosen to be $\rho/\sqrt{2}$ to have their intersections with the spherical inclusion take place where both the shear traction $\sigma_{r\theta}$ and the shear stress σ_{xy} is maximized on the circumference.

The normal stresses become dissipated by the wall friction k_s over a length $\lambda/2$ which we term the *secondary plastic zone*. Choosing coordinates x as shown in Fig. 8(a) the differential equation for the change of the normal stress along the cylinder is

$$\frac{d\sigma}{dx} - \frac{2\sqrt{2}\,k_s}{\rho} = 0 \qquad [7]$$

where

$$\sigma = E \frac{d\mu}{dx} \qquad [8]$$

The boundary conditions are $u = du/dx = 0$ at $x = 0$ (*i.e.*, $\sigma = 0$, at $x = 0$). which gives immediately

$$\sigma = \frac{2\sqrt{2}\, k_s}{\rho} x \qquad [9]$$

The extent of the secondary plastic zone is obtained from the displacement incompatibility at the interface, *i.e.*, $u = \gamma\rho/2$ at $x = \lambda/2$, and is

$$\frac{\lambda}{2} = \rho\sqrt{\frac{\gamma E}{2\sqrt{2}\, k_s}} \qquad [10]$$

This gives finally the interfacial tensile stress at $x = \lambda/2$ as

$$\sigma_{rr} = k_0 \left(1 + \sqrt{\frac{6\sqrt{6}}{m} \frac{\gamma}{\gamma_y}}\right), \qquad [11]$$

where the first term represents the contribution of the distant field and the second term the interfacial stress due to the secondary plastic zone. In Eq. [11] k_0 is the yield stress in shear of the polycrystal and m the well known Taylor factor, *i.e.*, $k_0/k_s = m/\sqrt{3}$, where m is generally taken as 3.1. This stress is again independent of size of the inclusion but increases relatively rapidly with increasing plastic strain as shown in Fig. 9. A cavity would form after a critical plastic strain γ_c when the interfacial stress equals the interfacial strength σ_i, *i.e.*, when

$$\gamma_c = \frac{\gamma_y m}{6\sqrt{6}} \left(\frac{\sigma_i}{k_0} - 1\right)^2. \qquad [12]$$

As discussed in Sec. 1.1 reaching the interfacial strength is necessary but not sufficient for cavity formation. The latter requires also that there be enough elastic energy stored in the region to provide for the energy of the free surfaces, *i.e.*, the ratio

$$\frac{(\alpha - \alpha_i)\pi\rho^2}{\beta\left(\frac{\sigma_i^2}{2E}\right)\left(\frac{2\pi\rho^3}{3}\right)} < 1 \qquad [13]$$

where the numerator is the surface energy of the cavity and the denominator the elastic energy that can be released by a cavity. In Eq. [13] α is the surface free energy of the cavity, α_i the interfacial energy, and the factor β of the order 0.5 is to account for the sharply decreasing tensile stress away from the interface. Considering that $(\alpha - \alpha_i) \approx \sigma_i b/4$ (where b is a lattice dimension), and that $\sigma_i/E \approx 0.1$ one finds that cavities can only open up when

$$\frac{\rho}{b} > \frac{3}{2} \frac{E}{\sigma_i} \approx 15. \qquad [14]$$

For weaker interfaces the critical size increases. For smaller inclusions stable cavities cannot form spontaneously: upon reaching of the interfacial strength the small inclusion will separate from the matrix a certain distance of atomic dimensions to relieve part of the elastic energy, but long range forces will still act across the interface. As already mentioned above, as straining continues and the displacement incompatibility between matrix and inclusions increases, the inclusion can still be slowly separated from the matrix in a gradual and stable manner. In some cases the inclusions may only be very poorly adhered to the matrix, and it can be assumed that $\sigma_i \approx 0$. Then the tensile incompatibility can be accommodated at the interface from the beginning by the formation of a cavity without punching out any secondary plastic zone.

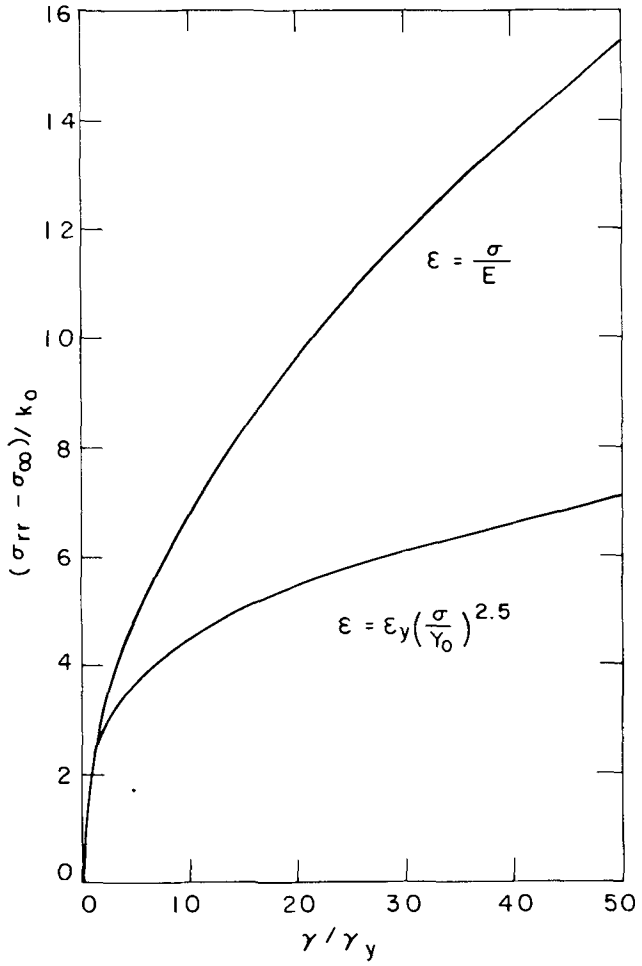

Fig. 9—Change of interfacial stress with increasing distant plastic strain for an elastic plug and a plastic, strain hardening plug.

To meet the condition given in Eq. [14] the inclusion must have a diameter of 75 to 100Å or over. For significantly larger inclusions it becomes more and more likely that some retained primary dislocations tangled around the inclusion act as sources and that the punched cylinder can undergo internal plastic relaxation as well.

b) Large spherical inclusions ($\rho \gg 100$Å): With internal plastic relaxation inside the punched cylinder the idealized model is still as shown in Fig. 8(*a*), giving rise to the same differential equation for the change in the normal stress σ by Eq. [7]. The stress-strain law now is non-linear and may be taken as

$$\frac{\epsilon}{\epsilon_y} = \frac{1}{\epsilon_y} \frac{du}{dx} = \left(\frac{\sigma}{Y_0}\right)^n \qquad [15]$$

where ϵ_y and Y_0 are the yield strain and yield stress in tension respectively, and where the exponent n can be anywhere from 2 to 8 representing decreasing capacities for strain hardening.

The solution of Eq. [7] together with the new non-

linear constitutive law, and the same boundary conditions as before can be obtained readily analytically for any exponent n and leads to (see Appendix)

$$\sigma_{rr} = k_0 \left[\left(\frac{\gamma}{\gamma_y} \right)^{\frac{1}{n}} + \sqrt{3} \left(\frac{\sqrt{6}\,(n+1)}{m} \frac{\gamma}{\gamma_y} \right)^{\frac{1}{n+1}} \right] \qquad [16]$$

where again the first term represents the contribution of the distant field. The secondary plastic zone now becomes

$$\frac{\lambda}{2} = \rho \frac{m}{2\sqrt{2}} \left(\frac{\sqrt{6}\,(n+1)}{m} \frac{\gamma}{\gamma_y} \right)^{\frac{1}{n+1}} . \qquad [17]$$

The increase of stress with plastic strain due to punching of the secondary plastic zone is now considerably slower than in the previous case where plastic relaxation inside the punched out cylinder was not possible. Fig. 9 shows the rise of the portion of the interfacial stress resulting from the punching of the secondary plastic zone for the case without relaxation and one where the hardening exponent $n = 2.5$ corresponding to copper. As the strain hardening rate becomes less with increasing exponents n, the rate of rise due to this component would become progressively less.

It is of interest to compare the above solution for the dislocation loop punching model with the continuum solution. When the hardening rate decreases as $n \rightarrow \infty$ the interfacial stress concentration goes asymptotically to

$$\lim_{n \rightarrow \infty} \left(\frac{\sigma_{rr}}{\sigma_\infty} \right) = 1 + \sqrt{3} \qquad [18]$$

This value is 89 pct higher than the lower limit given in Eq. [6] to which it should correspond. Although this solution is not to be preferred to the continuum solution discussed in the preceding section, it gives a result well within a factor of 2 of the latter, and will be useful to investigate effects of inclusion interaction.

c) Interacting Inclusions: Many investigators have reported that in a given sample large inclusions appear to produce cavities sooner than small ones—a particularly well reported case being that of Palmer and Smith.[19] Some of the previous explanations of this effect appear to be erroneous such as for instance the energy explanation of Gurland and Plateau[11] which was discussed above to be only a necessary condition for cavitation. The explanation advanced by Palmer and Smith that large inclusions may act as more efficient sinks for embrittling impurities could certainly be valid but cannot likely be responsible for this phenomenon in all cases. It is reasonable to expect that the effect may have its origin in interaction between inclusions. From dimensional analysis it is clear that the stress concentration cannot be dependent on inclusion size for the case of an isolated large inclusion (surface energy restrictions being unimportant) in an infinite medium where there is only one length dimension. When inclusions are in very finite media or when many inclusions are present in a body so that their spacing becomes of the order of their diameter a new length parameter appears in the analysis. It can be readily seen, however, that even in this case the stress concentration will be dependent only on the ratio of inclusion size to spacing. If all inclusions are of the same size this would make the stress concentration dependent only on the volume fraction of second phase but not directly on the inclusion size. It is clear, therefore, that an inclusion size dependence of the stress concentration can occur, at a given volume fraction of second phase, only if local variations of volume fraction exist, making it possible for some larger than average inclusions to be near neighbors at a spacing equal to or smaller than the average spacing. The situation is sketched out in Fig. 8(*b*) where the ratio of the net particle distance to the particle size is given by the local volume fraction c of second phase. Assuming that the interior of the punched cylinder of the secondary plastic zone can undergo plastic relaxation as in the previous case so that a constitutive equation of the type given in Eq. [15] is valid, the interfacial tensile stress can be calculated analytically for a fixed ρ/λ by the previously outlined approach only for an exponent of $n = 2$ (see Appendix). A much simpler approximate method can be used, however, to obtain the interfacial stress for any exponent n by breaking down the contributions to the interfacial stress into three sources: a) the strain hardening contribution resulting from the extension of the cylindrical zone as if it were an isolated tension specimen, b) the plastic drag contribution rising linearly from the center of the cylinder to the interface, and c) the contribution of the distant flow stress. This gives for the interfacial stress

$$\sigma_{rr} = k_0 \left[\sqrt{3} \left(\frac{\sqrt{3}\,(\gamma/\gamma_y)}{\sqrt{\frac{2\pi}{3c}} - \sqrt{\frac{8}{3}}} \right)^{\frac{1}{n}} + \frac{\sqrt{6}}{m} \left(\sqrt{\frac{2\pi}{3c}} - \sqrt{\frac{8}{3}} \right) + \left(\frac{\gamma}{\gamma_y} \right)^{\frac{1}{n}} \right] \qquad [19]$$

(see Appendix), where the well known expression (see, *e.g.*, Brown and Embury[34]) for the ratio of the net particle spacing to particle radius in a plane

$$\frac{\lambda}{\rho} = \sqrt{\frac{2\pi}{3c}} - \sqrt{\frac{8}{3}} , \qquad [20]$$

was used for a local volume fraction c of second phase. The change of the interfacial stress with increasing plastic strain is plotted in Figs. 10(*a*), and 10(*b*) for two values of n representing those for copper ($n = 2.5$) and steel, ($n = 4$) and for a variety of values of the volume fraction c. As can be seen from the figure for small volume fractions there is no interaction between inclusions.

We now consider first that all particles are of constant size but are distributed randomly in space or on any planar section. If the area allocated per particle is a, then the probability of finding n particles in an area of size A is given by a Poisson distribution as

$$P(n, a) = \frac{1}{n!} \left(\frac{A}{a} \right)^n \exp \left(- \frac{A}{a} \right). \qquad [21]$$

Considering that the chosen area A together with n corresponds to a new volume fraction

$$c = \frac{n\pi\rho^2}{A} \qquad [22]$$

for a particle radius of ρ, we can obtain readily the

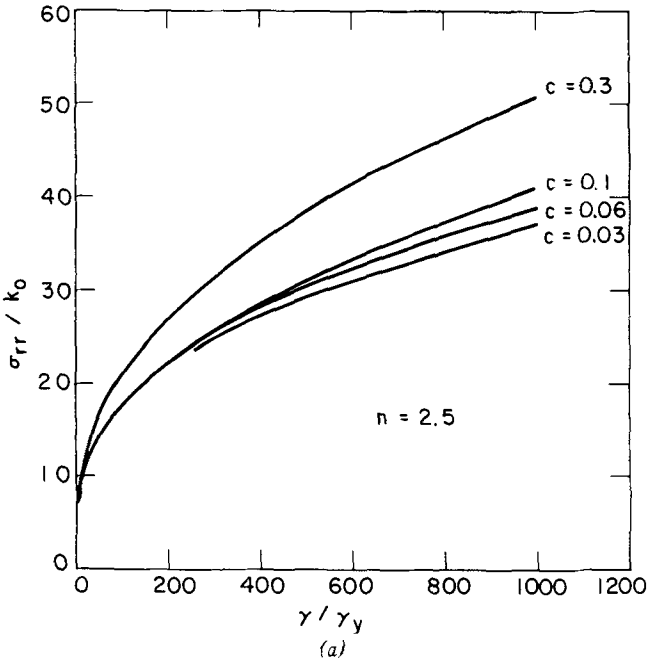

(a)

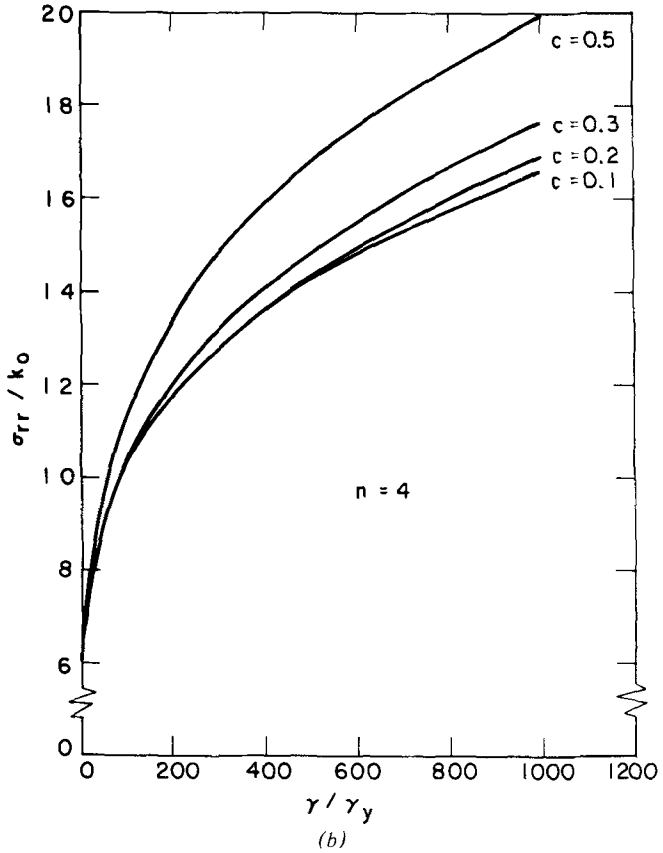

(b)

Fig. 10—Dependence of interfacial stress on local volume fraction of second phase particles, (*a*) for copper, $n = 2.5$, (*b*) for 1045 steel, $n = 4$.

probability for finding a local volume fraction c in *integer* multiples of the average volume fraction $\bar{c}$ by letting the area A go to a, *i.e.*,

$$P(c/\bar{c}) = \frac{1}{e}\left(\frac{\bar{c}}{c}\right)!, \quad \left(\frac{c}{\bar{c}} = 0, 1, 2, 3 \ldots\right) \qquad [23]$$

To obtain the probability for finding any arbitrary non-integer local volume fraction between c and $c + dc$ we merely let $n = c/\bar{c}$ become a continuous variable by introducing the gamma function to obtain

$$dP(c/\bar{c}) = \frac{dn/\Gamma(n+1)}{\int_0^\infty dn/\Gamma(n+1)} \quad \left(\text{where } n = \frac{c}{\bar{c}}\right). \qquad [24]$$

This leads finally to the probability of having a local volume fraction variation equal to or greater than c as,

$$1 - P(c/\bar{c}) = \frac{\int_{c/\bar{c}}^\infty dn/\Gamma(n+1)}{\int_0^\infty dn/\Gamma(n+1)} = 0.4412 \int_{c/\bar{c}}^\infty \frac{dn}{\Gamma(n+1)}, \qquad [25]$$

where the integrals in the numerator and denominator are the incomplete and complete Neumann functions which can be readily evaluated (see E. H. Erdelyi, et al.[35])

This probability is plotted in Fig. 11 as a function of the volume fraction ratio $c/\bar{c}$. To find the dependence of the plastic strain on the local volume fraction of second phase we equate the interfacial stress in Eq. [19] to the interfacial strength σ_i. With increasing plastic strain γ, the separation condition is reached first for closely spaced large inclusions (large local volume fraction of second phase) followed by inclusions with decreasing size and increasing spacing. The fraction f of the separated inclusions of the total population is then given directly by the cumulative probability of finding regions of local volume fraction having a value in excess of that for which the current plastic strain is sufficient for cavity formation, *i.e.*,

$$f(\gamma) = 1 - P(c/\bar{c}) = 1 - P(c/(\gamma)/\bar{c}). \qquad [26]$$

The application of this approach to inclusions in steel and copper is discussed in the accompanying paper by Argon and Im.[16]

Finally, it is of interest to prescribe when inclusions can be considered non-interacting, and when their interaction must be taken into account. Interaction between particles occur when the secondary plastic zones of neighboring particles in the plane of punching touch, *i.e.*, when λ/ρ of Eq. [17] equals that of Eq. [20]. This gives a critical strain ratio $(\gamma/\gamma_y)_{\text{crit.}}$ above which interactions must be considered.

$$\left(\frac{\gamma}{\gamma_y}\right)_{\text{crit.}} = \frac{m}{\sqrt{6}(n+1)}\left[\frac{\sqrt{2}}{m}\left(\sqrt{\frac{2\pi}{3c}} - \sqrt{\frac{8}{3}}\right)\right]^{n+1} \qquad [27]$$

The dependence of this critical strain on the volume fraction of second phase is shown in Fig. 12 for two strain hardening exponents.

2. EXPERIMENT

A direct experimental verification of the approximate analyses presented above was found desirable. Since no meaningful and reliable method of direct interfacial stress measurement could be conceived, it was considered useful to measure the plastic strain distribution around non-deforming inclusions to compare them with the strain distributions obtained for the limiting

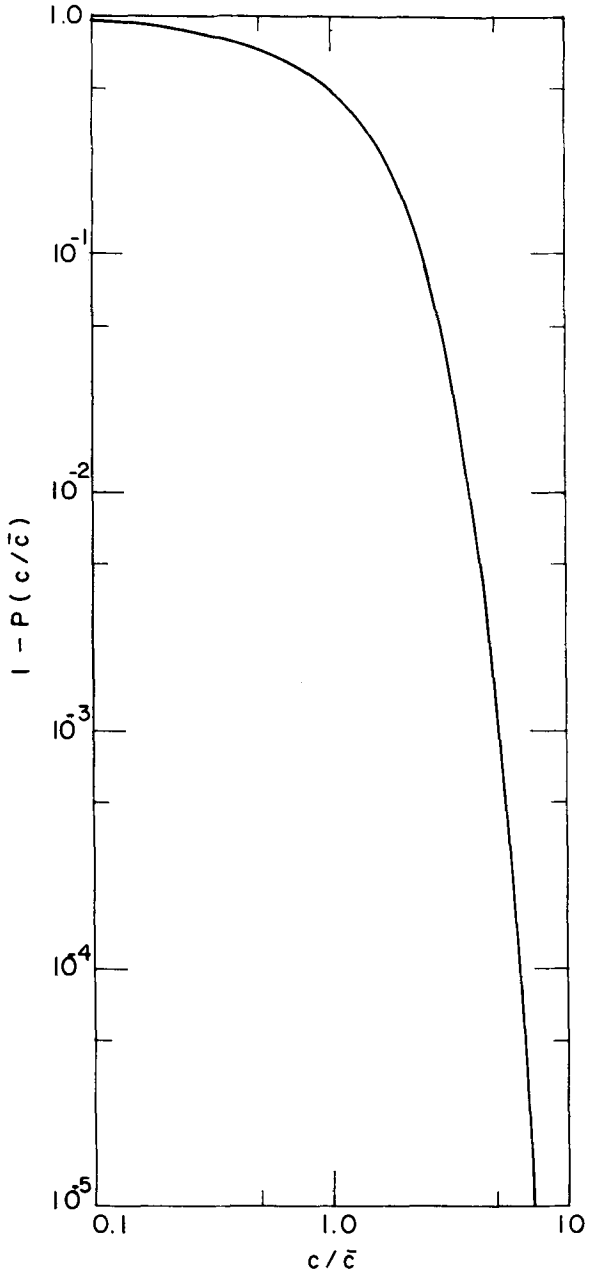

Fig. 11—Probability $(1 - P(c/\bar{c}))$ of finding a local volume fraction of second phase particles in excess of c, when the overall average is $\bar{c}$.

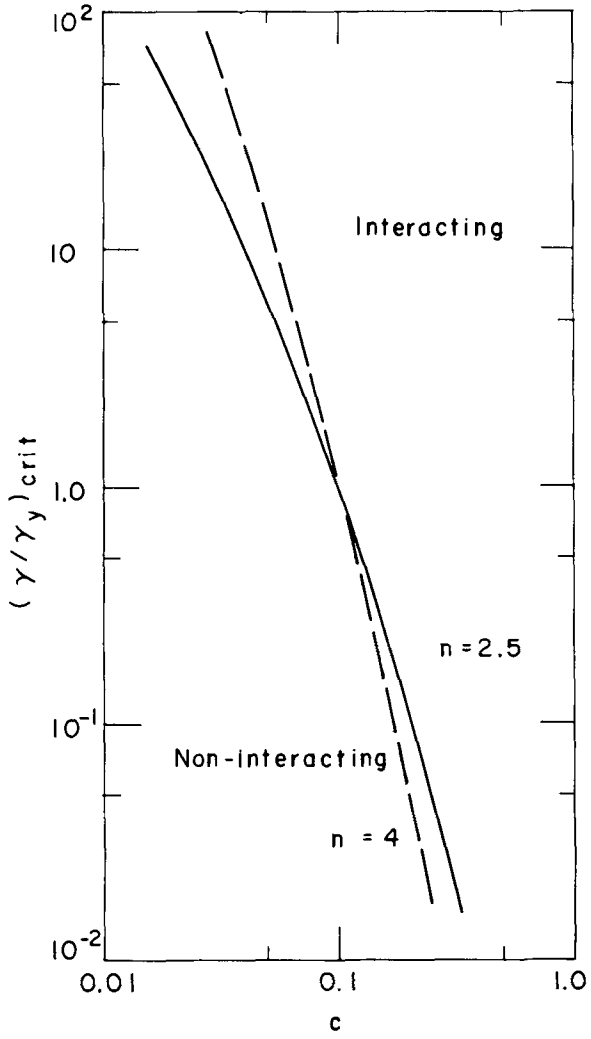

Fig. 12—The dependence of the critical strain ratio for particle interactions as a function of local volume fraction of second phase for two hardening exponents.

non-hardening and linear behaviors plotted in Fig. 6. To do this, a model experiment was designed in which the plastic strain distribution in a soft copper matrix could be measured around a hardened cylindrical copper-beryllium inclusion which could be heat treated to have a yield strength about 10 times that of the copper matrix. The model specimen was prepared by drilling a central 0.25 in. hole almost through a 2.5 in. diam OFHC copper cylinder. This piece together with a graphite funnel containing an amount of castable charge of Cu-Be alloy was placed into a vacuum furnace where the specimen and the inside of the drilled hole was evaporation-cleaned by maintaining the assembly 100°C below the solidus point of the alloy for 45 min. The temperature was then raised to cast the charge in place. After this the specimen was cooled to 800°C and maintained there for two h to homogenize the alloy followed by quenching and tempering at 300°C for two h to obtain peak hardness. The cylindrical bar with the Cu-Be core was then machined into two 1.75 in. square blocks of 1.5 in. thickness with the cylindrical core running along the short length and through the center of the square faces. All faces of the blocks were then polished and one of the square faces was provided with a fine, scratched square grid of 0.017 in. spacing running parallel to the edges of the block. The two blocks were then put together face to face so that the grid remained between the blocks. The pair were then compressed 10 pct in a plane strain compression jig as shown in Fig. 13. The compression faces and the two outside faces touching the jig were coated with a MoS_2 spray to reduce friction. This prevented barelling of the specimen. After compression the blocks were removed from the jig, taken apart to reveal the internal grid, which was then measured to compute the distribution of the lateral strain parallel to the principal extension direction. This distribution of the measured normal strains is shown in Fig. 6 for comparison with the theoretically determined bounds for the strain distribution. The actual measured strains are greater than the plastic strains near the inclusion but become smaller than the plastic strains at greater

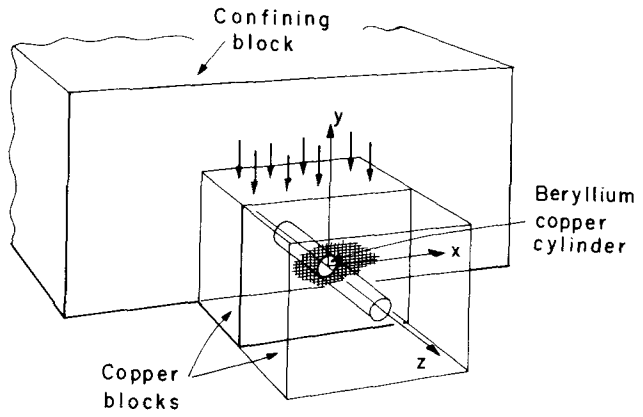

Fig. 13—Experimental arrangement for determining local plastic strains in a copper block with a hardened, cylindrical Cu-Be "inclusion".

distances. Since the inclusion was not rigid but actually had a fairly high compliance and showed signs of some plastic straining these departures from expected behavior are considered not surprising. In any event the experimental distribution lies nearer to the plastic non-hardening solution than to the linear solution. This lends support to the bounding analysis discussed in Sec. 1.2.

3. DISCUSSION

The various approximate analyses presented above show that for very small inclusions where no local diffuse plastic relaxation is possible because of the complete absence of dislocations in the surroundings, the shear stresses on the inclusion interface can be relieved by punching out dislocation loops as suggested by Ashby.[14] This cannot relieve the interfacial tensile stresses which may reach the interfacial strength. When the inclusion diam is less than about 100Å there is insufficient elastic energy stored in the surroundings of the inclusion and cavities cannot form upon reaching of the interfacial strength at the interface. When the inclusion diam exceeds this cut-off limit, stable cavities can form. In this range of increasingly larger inclusions, however, local plastic relaxations become more and more likely and a continuum analysis for the stress concentrations becomes appropriate. All such continuum analyses give a rather mild stress concentration factor which for a pure shear mode of deformation is only of the order of $\sqrt{3}$, *i.e.*, the interfacial stress is of the order of the local equivalent flow stress in tension. When the volume fraction of second phase is small so that the secondary plastic zones of particles do not touch, then the particles act in isolation and the interfacial stress is independent of the particle size but depends only on the local flow stress and any local long range triaxial stress. When the volume fraction is large or when the shear strain is large so that the secondary plastic zones of particles touch, the particles interact. If the particles are of uniform size and quasi-uniform spacing, the interfacial stress becomes in addition to the plastic strain, dependent also on the volume fraction of the second phase but remains still independent of the particle size, *i.e.*, at constant volume fraction any increase in particle size is balanced by a proportional increase in particle spacing. The interfacial stress becomes particle size dependent only if there are significant local variations of volume fraction of second phase from point to point for a given average second phase volume fraction. Such variations of volume fraction actually exist in many inclusion bearing alloys and can account for the often reported effects of particle size on local strain for cavity formation in the case of non-deformable inclusions. Experimental evidence for such effects will be presented in the accompanying paper by Argon and Im.[16]

The interaction of secondary plastic zones around particles discussed here is, however, not the only possible explanation for particle size effects in void formation. Cox and Low[36] have discussed other possibilities for plastically deformable inclusions and for brittle, inclusions, having a variability of strength based on statistically distributed flaws.

We close with a note of caution that our analysis applies only to nearly non-deformable, equiaxed inclusions. Therefore the results must not be applied indiscriminately to cases of deformable inclusions which could present qualitatively different behavior.

APPENDIX

A.1. Interfacial Stresses Around Large Spherical Inclusions

The first integral of the differential equation for the normal stress along the secondary plastic zone (Eq. [7]), gives

$$\sigma(x) = \frac{2\sqrt{2}\,k_s}{\rho}\,x + C \qquad [A\text{-}1]$$

where x is measured from the end of the secondary plastic zone. Using the non-linear constitutive equation of Eq. [15] gives

$$\frac{\epsilon}{\epsilon_y} = \left(\frac{2\sqrt{2}\,k_s x}{Y_0\rho} + \frac{C}{Y_0}\right)^n \qquad [A\text{-}2]$$

which when integrated gives the displacement u, also measured from the end of the secondary plastic zone as

$$u = \frac{\epsilon_y Y_0 \rho}{2\sqrt{2}\,k_s(n+1)}\,\xi^{n+1} + D \qquad [A\text{-}3]$$

where

$$\xi = \frac{2\sqrt{2}\,k_s x}{Y_0\rho} + \frac{C}{Y_0} \qquad [A\text{-}4]$$

When $x = 0$, $\xi = C/Y_0$ and $u = 0$. This gives

$$u = \frac{\epsilon_y Y_0 \rho}{2\sqrt{2}\,k_s(n+1)}\left[\left(\frac{2\sqrt{2}\,k_s x}{Y_0\rho} + \frac{C}{Y_0}\right)^{n+1} - \left(\frac{C}{Y_0}\right)^{n+1}\right] \qquad [A\text{-}5]$$

The other boundary condition is that $u = \gamma\rho/2$ when $x = \lambda/2$. This gives

$$\frac{\gamma\rho}{2} = \frac{\epsilon_y Y_0 \rho}{2\sqrt{2}\,k_s(n+1)}\left[\left(\frac{\sqrt{2}\,k_s \lambda}{Y_0\rho} + \frac{C}{Y_0}\right)^{n+1} - \left(\frac{C}{Y_0}\right)^{n+1}\right] \qquad [A\text{-}6]$$

from which the integration constant C could be deter-

mined as a function of the yet unknown extent of the secondary plastic zone $\lambda/2$. The secondary plastic zone can then be obtained by substituting $C(\lambda/2)$ into Eq. [A-1] and setting $\sigma = 0$ at $x = 0$. This, however, tells immediately that $C = 0$, which can only be satisfied if λ is chosen to satisfy Eq. [A-6] for the special value of $C = 0$. This gives the extent of the secondary plastic zone as

$$\frac{\lambda}{2} = \frac{\rho}{2\sqrt{2}} m \left(\frac{\sqrt{6}\,(n+1)}{m} \frac{\gamma}{\gamma_y}\right)^{\frac{1}{n+1}} \qquad [A\text{-}7]$$

where $m = \sqrt{3}\,k_0/k_S$ and $\epsilon_y = \gamma_y/\sqrt{3}$ was used in the evaluation.

We now obtain the interfacial stress due to the punching out of the secondary plastic zones as

$$\sigma = k_0\sqrt{3}\left(\frac{\sqrt{6}\,(n+1)}{m}\left(\frac{\gamma}{\gamma_y}\right)\right)^{\frac{1}{n+1}} \qquad [A\text{-}8]$$

The distant stress governing the distant plastic strain will also appear across the boundary and must be added to the above stress to obtain the total interfacial stress. This stress is $k_0(\gamma/\gamma_y)^{1/n}$ giving for the total interfacial tensile stress σ_{rr} finally,

$$\sigma_{rr} = k_0\left[\left(\frac{\gamma}{\gamma_y}\right)^{\frac{1}{n}} + \sqrt{3}\left(\frac{\sqrt{6}\,(n+1)}{m}\frac{\gamma}{\gamma_y}\right)^{\frac{1}{n+1}}\right] \qquad [A\text{-}9]$$

A.2. Interacting Inclusions

When the secondary plastic zones of particles touch at large volume fractions of second phase, or at large plastic strains, the interfacial stress becomes dependent also on the local volume fraction of second phase. For this case analytical solutions are difficult to obtain and it is more instructive to resort to approximate solutions. An approximate solution can be obtained readily by dividing the interfacial stress up into three parts. The first contribution to the interfacial stress comes from considering the cylindrical interconnecting plastic zone between particles as shown in Fig. 8(*b*) as a round tensile bar which has undergone a plastic extensional strain of $\gamma\rho/\lambda$ which results in a stress of

$$\sigma_1 = Y_0\left(\frac{\epsilon}{\epsilon_y}\right)^{\frac{1}{n}} = \sqrt{3}\,k_0\left(\frac{\rho}{\lambda}\frac{\gamma}{\gamma_y}\sqrt{3}\right)^{\frac{1}{n}} \qquad [A\text{-}10]$$

The second contribution comes from the plastic shear drag on the extending cylinder along its walls which is

$$\sigma_2 = k_S\sqrt{2}\left(\frac{\lambda}{\rho}\right) \qquad [A\text{-}11]$$

where the shear drag along the wall $k_S = \sqrt{3}\,k_0/m$, can be taken as the critical resolved shear stress for slip in a single crystal, which is the polycrystal yield strength in shear k_0 divided by the Taylor factor for shear, *i.e.*, $m/\sqrt{3} = 3.1/\sqrt{3}$.

The third contribution comes from the boundary tractions governing the distant field. This contribution is

$$\sigma_3 = k_0(\gamma/\gamma_y)^{\frac{1}{n}} \qquad [A\text{-}12]$$

The sum of all three contributions gives the total interfacial tensile stress and is the quantity in Eq. [19].

An analytical solution for the dislocation loop punching component of the interfacial stress, *i.e.*, components 1 and 2 above, can be obtained again readily for $n = 2$, by substituting Eq. [A-6] into Eq. [A-1] and letting $x = \lambda/2$. This would give the interfacial stress as a function of λ/ρ which now, as shown in Fig. 8(*b*) is governed by the local concentration of second phase c. The end result is obtained readily as

$$\sigma_{rr} = k_0\left[\left(\frac{\gamma}{\gamma_y}\right)^{1/2} + \frac{\sqrt{6}}{2m}\left(\frac{\lambda}{\rho}\right) \times\left(1 + \sqrt{\frac{2\sqrt{3}\,m^2\,(\gamma/\gamma_y)}{(\lambda/\rho)^3} - \frac{1}{3}}\right)\right] \qquad [A\text{-}13]$$

where

$$\frac{\lambda}{\rho} = \sqrt{\frac{2\pi}{3C}} - \sqrt{\frac{8}{3}} \qquad [A\text{-}14]$$

is the ratio of the net distance in the plane of plastic punching to the radius of the particle.

For other n values an approximate solution of the equations in Appendix A.1 is possible for the interacting particles. For given values of (γ/γ_y), (λ/ρ), and n, the value of C/Y_0 can be obtained from Eq. [A-6] by curve plotting. The interfacial stress resulting from the first two contributions can then be obtained from Eq. [A-1] for $x = \lambda/2$. To this the contribution from the distant field given by Eq. [A-12] must still be added. Interfacial stresses obtained in this somewhat more exact manner are usually about 5 pct smaller than those computed from Eqs. [19] and [20].

ACKNOWLEDGMENTS

We are indebted to Professors F. A. McClintock and M. F. Ashby for many useful comments, to Dr. D. K. Brown for showing us his then unpublished solution for stresses and strains around inclusions and to Dr. J. Carson for initial help in computation. This work was supported initially by NSF under grant GK 1875X and later by ARPA under Contract No. DAHC15-70C-D283.

REFERENCES

1. J. Henry: *Proc. Amer. Assoc. Advancement Science,* 1855, vol. 9, p. 102.
2. W. A. Backofen: *Met. Trans.,* 1973, vol. 4, p. 2679.
3. K. E. Puttick: *Phil. Mag.,* 1959, vol. 4, p. 964.
4. E. Orowan: *Rept. Progr. Phys.,* 1949, vol. 12, p. 185.
5. A. R. Rosenfield: *Met. Rev.,* 1968, vol. 13, no. 121, p. 29.
6. F. A. McClintock: *Fracture,* H. Liebowitz, ed., vol. 3, p. 106, Academic Press, New York, 1971.
7. J. R. Rice, and D. M. Tracey: *J. Mech. Solids,* 1969, vol. 17, p. 201.
8. C. A. Berg: *Inelastic Behavior of Solids,* M. F. Kanninen *et al.*, eds., p. 171, McGraw-Hill, New York, 1970.
9. F. A. McClintock: *Physics of Strength and Plasticity,* A. S. Argon, ed., p. 307, M.I.T. Press, Cambridge, Mass., 1969.
10. R. O. Ritchie, J. F. Knott, and J. R. Rice: *J. Mech. Phys. Solids,* 1973, vol. 21, p. 395.
11. J. Gurland and J. Plateau: *Trans. ASM,* 1963, vol. 56, p. 442.
12. K. Tanaka, T. Mori, and T. Nakamura: *Phil. Mag.,* 1970, vol. 21, p. 267.
13. D. Broek: "A Study on Ductile Fracture," Ph.D. Thesis, Delft, Netherlands, 1971.
14. M. F. Ashby: *Phil. Mag.,* 1966, vol. 14, p. 1157.
15. F. A. McClintock: *Ductility,* p. 255, ASM, Metals Park, Ohio, 1968.
16. A. S. Argon and J. Im: *Met. Trans. A,* 1975, vol. 6A, pp. 839-51.

17. F. A. McClintock: *J. Appl. Mech.*, 1968, vol. 35, p. 363.
18. I. G. Palmer and G. C. Smith: *Proc. Second Bolton Landing Conf. on Oxide Dispersion Strengthening*, p. 253, Gordon and Breach, N.Y., 1968.
19. J. Gurland: *Acta Met.*, 1972, vol. 20, p. 735.
20. L. M. Brown and W. M. Stobbs: *Phil. Mag.*, 1971, vol. 23, p. 1201.
21. A. N. Stroh: *Proc. Roy. Soc.*, (London), 1955, vol. A232, p. 548.
22. C. Zener: *Fracturing of Metals*, p. 3, ASM, Metals Park, Ohio, 1949.
23. A. N. Stroh: *Proc. Roy. Soc.*, (London), 1954, vol. A223, p. 404.
24. M. F. Ashby: private communication, 1971, (formerly at Harvard University, now at University Engineering Laboratory, Cambridge University, Cambridge, U.K.).
25. P. B. Hirsch and F. J. Humphreys: *Physics of Strength and Plasticity*, A. S. Argon, ed., p. 189, M.I.T. Press, Cambridge, Mass., 1969.
26. W. C. Huang: *Int. J. Solids, Structures*, 1971, vol. 8, p. 149.
27. J. Orr and D. K. Brown: *Elasto-Plastic Solution for a Cylindrical Inclusion in Plane Strain*, Dept. of Mech. Eng. Report, University of Glasgow, 1973.
28. S. S. Rhee and F. A. McClintock: *Proc. Fourth U.S. Nat. Cong. Appl. Mech.*, vol. 2, p. 1007, ASME, New York, 1962.
29. B. V. Marcal and I. P. King: *Int. J. Mech. Sci.*, 1967, vol. 9, p. 143.
30. N. I. Muskhelishvilli: *Some Basic Problems of the Mathematical Theory of Elasticity*, p. 355, P. Noordhoff Ltd., Groningen, Netherlands, 1963.
31. G. N. Savin: *Stress Concentration Around Holes*, p. 260, Pergamon Press, N.Y., 1961.
32. J. D. Eshelby: *Proc. Roy. Soc.*, (London), 1957, vol. A241, p. 376.
33. A. Kelly, W. R. Tyson, and A. H. Cottrell: *Phil. Mag.*, 1967, vol. 15, p. 567.
34. L. M. Brown and J. D. Embury: *Abstracts, Third International Conference on Strength of Metals and Alloys*, Institute of Metals, London, 1973.
35. A. Erdelyi, W. Magnus, F. Oberhettinger, and F. G. Tricomi: *Higher Transcendental Functions*, vol. 3, p. 217, McGraw-Hill, New York, 1955.
36. T. B. Cox and J. R. Low, Jr.: *Met. Trans.*, 1974, vol. 5, p. 1457.